Ultrasound in Med. & Biol., Vol. 00, No. 00, pp. 1–6, 2018

0301-5629/$ - see front matter

https://doi.org/10.1016/j.ultrasmedbio.2018.06.008

● *Technical Note*

A LUNG PHANTOM MODEL TO STUDY PULMONARY EDEMA USING LUNG ULTRASOUND SURFACE WAVE ELASTOGRAPHY

JINLING ZHOU, and XIAOMING ZHANG
Department of Radiology, Mayo Clinic, Rochester, Minnesota, USA

(*Received* 11 *January* 2018; *revised* 4 *June* 2018; *in final from* 13 *June* 2018)

Abstract—Lung ultrasound surface wave elastography (LUSWE) is a novel technique used to measure superficial lung tissue stiffness. A phantom study was carried out in the study described here to evaluate the application of LUSWE to assess lung water for pulmonary edema. A lung phantom model with cellulose sponge was used; various volumes of water were injected into the sponge to model lung water. Shaker-generated surface wave propagation on the sponge surface was recorded by a 10-MHz ultrasound probe at three shaker frequencies: 100, 150 and 200 Hz. Surface wave speeds were calculated but did not exhibit dependence on the volume of injected water. However, the shear viscosity of the sponge increased with water content, and shear elasticity also exhibited a subtle increase. This study suggests that sponge viscoelasticity might change with the water content, which can be detected by LUSWE. (E-mail: zhang.xiaoming@mayo.edu) **© 2018 World Federation for Ultrasound in Medicine & Biology. All rights reserved.**

Key Words: **Lung ultrasound surface wave elastography, Surface wave speed, Pulmonary edema, Lung phantom, Viscoelasticity.**

INTRODUCTION

Pulmonary edema is a fundamental feature of congestive heart failure and inflammatory conditions such as acute respiratory distress syndrome (Picano and Pellikka 2016). A high extravascular lung water (EVLW) level predicts severe prognosis in critically ill patients (Sakka et al. 2002) and increased risk of death or rate of heart failure re-admission (Coiro et al. 2015). Assessment of EVLW, however, is challenging. Chest X-ray and chest computed tomography (CT) have been the historical standards in the assessment of EVLW, but these imaging studies require ionizing radiation and radiology facilities and pose a significant logistic burden. Because of the high levels of X-ray absorption by bones, the image quality of chest X-ray is also mediocre. Researchers are actively searching for other methods.

Ultrasound is not traditionally used to evaluate the lung. In normal aerated lungs, most of the ultrasound energy is reflected from the lung surface because of the large acoustic impedance difference between the pleural lining of the lung and the air within the lung. In the presence of EVLW, however, the ultrasound beam finds subpleural interlobular septa thickened by edema (Gargani 2011). The reflection of the ultrasound beam produces reverberation artifacts, called "B-lines," in wet lungs. These B-lines start from the plural line and extend to the edge of the screen looking like comet tails. The location and amount of B-line artifacts in ultrasound images (Corradi et al. 2016; Lichtenstein and Mezière 1998) are used to evaluate pulmonary edema (Picano et al. 2006) and congestive heart failure (Cardinale et al. 2014). A recent multicenter trial found that lung ultrasound (LUS) was more sensitive than chest X-ray for the diagnosis of cardiogenic pulmonary edema (Pivetta et al. 2015). However, analysis of B-line artifacts is qualitative and relies on visual interpretation, which is subject to inter-operator variability (Corradi et al. 2016).

We have developed a novel technique, lung ultrasound surface wave elastography (LUSWE), to measure superficial lung tissue elastic properties (Zhang et al. 2011, 2016, 2017, 2018). LUSWE measures the lung surface wave by recording thousands of lung ultrasound images. In addition to lung ultrasound's qualitative evaluations, LUSWE can also quantitatively characterize the lung. In LUSWE, a 0.1-s harmonic vibration at a given frequency is generated by the indenter of a handheld vibrator on the chest wall of a subject. The ultrasound

Address correspondence to: Xiaoming Zhang, Department of Radiology, Mayo Clinic, 200 First Street SW, Rochester, MN 55905, USA. E-mail: zhang.xiaoming@mayo.edu

probe is positioned about 5 mm away from the indenter in the same intercostal space to measure the surface wave propagation generated on the lung in that intercostal space. The surface wave speed of lung is determined from the change in wave phase with distance and is not dependent on the location of wave excitation. LUSWE has been reported to successfully differentiate the lung elastic properties of patients with interstitial lung disease and healthy controls (Zhang et al. 2017). The objective of this research was to evaluate preliminarily whether LUSWE could be used to measure the EVLW level for pulmonary edema through a lung phantom model study.

METHODS

Sponges have been used as a lung phantom in past research studies (Molinari et al. 2014; Soldati et al. 2011). In particular, Blüthgen et al. (2017) reported that sponges can reproduce nicely the commonly observed lung ultrasound A- and B-line artifacts and can be used for relevant lung studies. In our experiment, we used a rectangular cellulose sponge for our lung phantom model. Tap water was injected by syringe at three locations approximately 2 cm apart in the middle of the sponge surface. The experimental setup is illustrated in Figure 1. The purple sponge (Ocelo Utility Sponge, 3M, St. Paul, MN, USA), with a labeled size of $15.2 \times 9.1 \times 2.2$ cm, is the lung phantom sponge for measurement. Diameters of the pores on this sponge vary from sub-millimeter to a few millimeters. Tiny sub-millimeter pores are distributed all over the walls of larger pores. Beneath the purple sponge, a large pink sponge and a piece of black rubber were added as cushions to reduce the strength of the wave reflected from the boundaries. This setup can help generate the surface wave propagation and avoid other types of waves such as the Lamb wave in a contained structure. We previously proposed a concept of start frequency for generating the surface waves in a finite phantom structure (Zhang 2016). We found that different standing wave modes were generated below the start frequency because of wave reflection. However, pure symmetric surface waves were generated from the excitation above the start frequency. By use of the wave speed dispersion above the start frequency, the viscoelasticity of the phantom can be correctly estimated. By reduction of the wave reflection and measurement of surface wave speed above the start frequency, surface wave propagation can be generated in a finite structure. A shaker (Model FG-142, Labworks Inc., Costa Mesa, CA, USA) was placed in contact with the sponge to generate harmonic vibrations on the sponge surface. Three vibration frequencies (100, 150 and 200 Hz) were used, and the duration for each was 0.1 s. An ultrasound probe (Verasonics linear

Fig. 1. Experimental setup. An ultrasound probe was placed atop an ultrasound gel pad to measure the surface wave speed of the lung phantom—the purple sponge. The pink sponge and the black rubber were placed under the purple sponge to reduce the reflection of the sound wave from harder surfaces. A shaker was in contact with the purple sponge surface to generate harmonic vibrations on the sponge surface. The bars behind the shaker and the ultrasound probe are the holder frames used to keep the equipment in place.

transducer L11-4 V, Verasonics Inc., Kirkland, WA, USA) with a frequency of 10 MHz was placed about 0.5 cm away from the shaker to detect the waves propagated on the sponge surface. An Aquaflex ultrasound gel pad (04-02, Parker Laboratories, Inc. Fairfield, NJ, USA) was placed between the ultrasound probe and the purple sponge to create a separation for wave detection, because ultrasound locates an object by multiplying the speed of sound by the length of time it travels to the object. The ultrasound measurement and shaker vibrations were synchronized by a vantage ultrasound system (Vantage 256, Verasonics Inc.), and the B-mode images generated were collected for further analysis.

The waves generated by the shaker will travel at the shaker frequency. Through analysis of the phase change $\Delta\phi$ over a distance of Δr at the sponge surface, the surface wave speed C_s can be determined with the known angular shaker frequency ω: $C_s = \omega|\Delta r/\Delta\phi|$ (Zhang et al. 2016). The accuracy of calculation can be greatly improved by incorporating multiple locations.

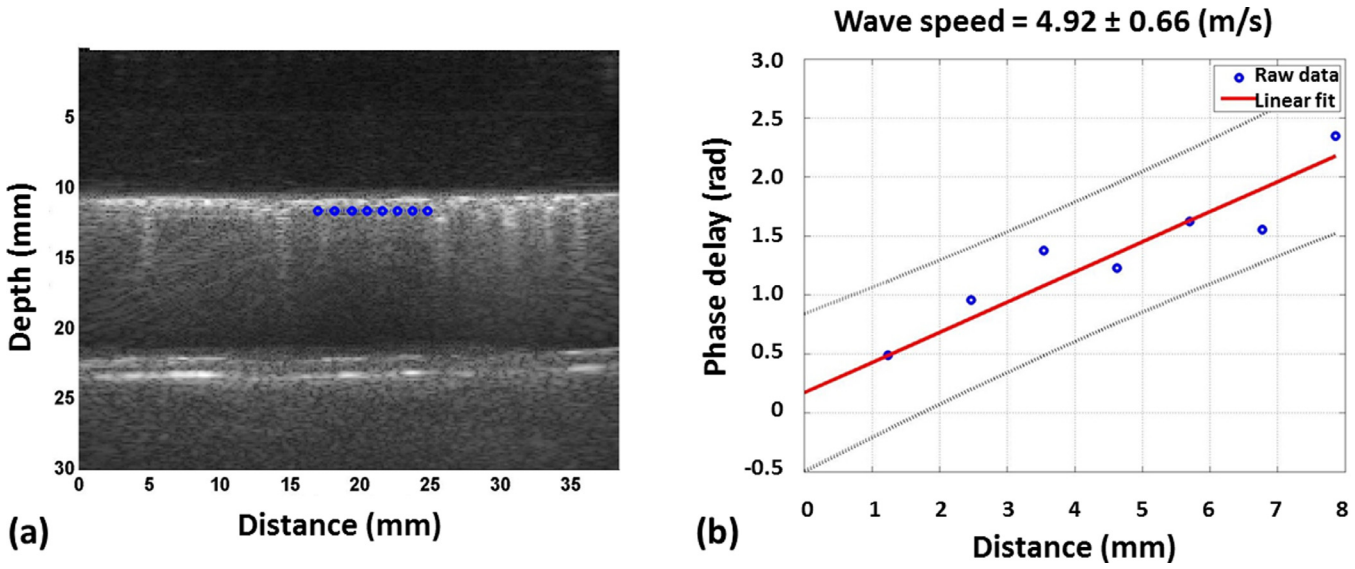

Fig. 2. (a) Typical B-mode image collected from our experiment. Eight locations were selected on the sponge surface for further analysis and are marked in *blue*. (b) Regression process. The x- and y-axes are the distance and phase delay of each location relative to the first location. The best-fit slope of the graph is thus the rate at which the phase changes with distance. *Blue dots* are the data points read from (a). The *red line* is the best linear fit for the graph. Surface wave speed was calculated by dividing angular shaker frequency by the rate at which the phase changes with distance.

Figure 2a is the ultrasound image of a sponge injected with 6 mL water. The upmost bright horizontal line is the top surface of the purple sponge. The gel pad appeared dark above the purple sponge. The lower *bright horizontal lines* are the bottom surface of the purple sponge and the top surface of the pink sponge. The *vertical lines* starting at the purple sponge surface and extending all the way below until blurry are the B-line artifacts observed frequently in pulmonary edema patients. These B-line artifacts were observed for all wet sponges, but not for the dry sponge. Eight locations were selected and marked in *blue* along the top surface of the purple sponge for surface wave speed calculation. The linear regression model $\hat{\Delta\phi} = -\alpha\Delta r + \beta$ was used to better estimate the $\Delta r/\Delta\phi$ ratio among these locations, for which $\hat{\Delta\phi}$ is the linear regression of $\Delta\phi$, and α and β are the regression coefficients. Figure 2b illustrates the regression process. The x- and y-axes are the distance and phase delay for each location relative to the first selected location. A linear curve was used to fit the data. The slope coefficient α from the best-fit line is the best estimation of the rate at which the phases increase with distance. The surface wave speed can therefore be simplified as $C_s = \omega/\alpha$. Figure 2b illustrates that the surface wave speed here is 4.92 m/s with an uncertainty of 0.66 m/s.

With the surface wave speeds measured at several frequencies, the material viscoelasticity can be estimated (Zhang et al. 2016) as

$$C_s = \sqrt{\frac{2\left(\mu_1^2 + \omega^2\mu_2^2\right)}{\rho\left(\mu_1 + \sqrt{\mu_1^2 + \omega^2\mu_2^2}\right)}} \quad (1)$$

where μ_1 is shear elasticity, μ_2 is shear viscosity, ω is angular frequency $2\pi f$ and ρ is material density. The total weight of the sponge after each water injection was measured with a scale (Mettler Toledo PB302 precision balance, Mettler-Toledo GmbH, Laboratory & Weighing Technologies, Greifensee, Switzerland) with a reading accuracy of 0.1 g. Sponge volume was measured when the sponge was completely dry and when it was injected with 15 mL of water. Volumes for sponges with water content <15 mL were estimated based on these two end volumes. Sponge densities were therefore the divisions of total weight over the estimated volumes. Using known wave speeds and material densities, we were able to estimate the viscosity and elasticity of sponge with different water contents by fitting eqn (1) to the experimental data.

RESULTS AND DISCUSSION

The purple sponge was measured when it was dry and after water was injected into it with a syringe. For each additional measurement, 1 mL of water was propelled from the syringe to each of the three locations in the middle of the sponge surface. We added water five times and acquired six sets of measurements. Figure 3 plots the calculated surface wave speeds for the six cases at three shaker frequencies. Baseline data, represented by the slanted-line column, are for the dry sponge. The different-colored columns represent sponges containing different volumes of water. The exact volume of water for each measurement is given in the figure legend after the corresponding color. Because each measurement was repeated three times, the final surface wave speeds were the averages of three repeated measurements; uncertainties, similarly, were the averages of three uncertainties from individual analysis of the repeated measurements. These uncertainties are represented by the *black vertical error lines* at the tops of the colored bars. As illustrated in the graph, surface wave speed increased with shaker frequency, similar to the patient study results obtained with LUSWE (Zhang et al. 2017). But the surface wave speeds for sponges injected with different volumes of water exhibited no dependence on the water volume; instead, they fluctuated around similar values for each shaker frequency. This indicates that the differences induced by water do not change surface wave speeds.

Table 1 summarizes the total weight and density of the sponge at different water contents. Because of the light weight of the sponge, overall sponge density was doubled when 15 mL of water was injected. With the material densities and known surface wave

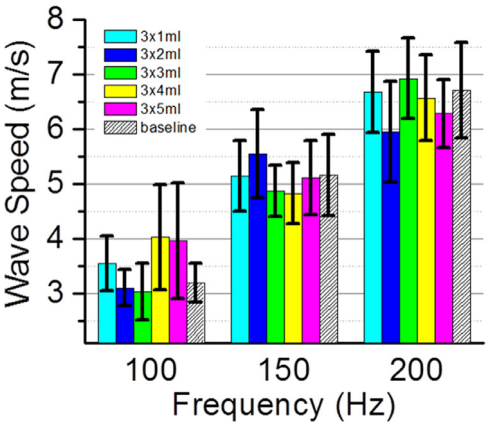

Fig. 3. Sponge surface wave speeds obtained for six sponge conditions at three shaker frequencies: 100, 150 and 200 Hz. The baseline was measured when the sponge was dry and is represented by the slanted-line column. Water was added in increments of 1 mL at three locations in the middle of the purple sponge surface. The total volume of water added is given the legend after each color code. Uncertainties are represented by *black vertical bars*. Although surface wave speed increased with shaker frequency, the data for different sponge conditions were similar at each shaker frequency.

Table 1. Total weight and average density of sponges containing different volumes of water

Water injected (ml)	Total weight (g)	Sponge density (kg/m^3)
0	14.04	74.3
3	17.17	89.4
6	20.31	104.0
9	23.4	117.9
12	26.18	129.8
15	29.23	142.7

speeds, the shear viscosity and elasticity were estimated using eqn (1). Starting with initial guesses, the shear viscosity and elasticity were adjusted until the differences between the calculated surface wave speeds and experimental values were minimized. The best-fit shear viscosity and elasticity obtained for the averaged surface wave speeds are plotted as *red dots* and black *squares* in Figure 4 for sponges with different water contents. The uncertainties of these values were estimated by the fitted results for the highest and lowest surface wave speeds for each measurement. Because of the non-linear dependence of surface wave speeds on viscoelasticity, the error lines were not symmetric around the fitted results for the averaged surface wave speeds. As illustrated in Figure 4, the shear viscosity of the sponge increased with the increase in water content, and the increase in shear elasticity was subtle. Because the sponge is lightweight, we observed the increase of the sponge viscoelastcity with water, whereas the sponge surface wave speeds stayed at relatively similar levels after water injection.

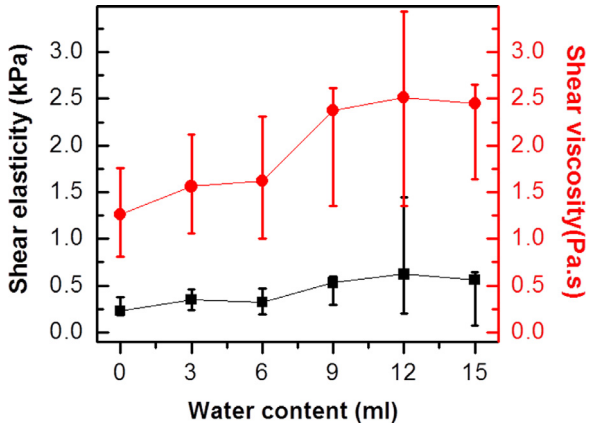

Fig. 4. Viscoelasticity of the purple sponge with different water volumes. *Black data points* represent shear elasticity, and *red data points*, shear viscosity. *Black squares* and *red dots* represent fitted results from the averaged surface wave speeds. Ranges of uncertainties are defined by the fitted results for the highest and lowest possible surface wave speeds for each measurement. Because of the non-linear dependence of the surface wave speeds on viscoelasticity, the error bars for viscoelasticity are not symmetric.

CONCLUSIONS

A lung phantom study was carried out to test the feasibility of applying LUSWE to measure water content. Measurements were taken at six stages of the lung phantom: completely dry and injected with 3, 6, 9, 12 and 15 mL of water. B-Line artifacts were not present in the dry sponge images, but appeared once the water was added, representing a normal lung and diseased lungs with pulmonary edema. The calculated sponge surface wave speeds were generally larger at higher shaker frequencies, which mimicked the LUSWE measurements on human lung. The surface wave speeds for the six stages of the lung phantom, however, appear to be similar. By fitting the measured surface wave speeds to a theoretical model (eqn [1]) of surface wave speed dependence on viscoelasticity, the shear elasticity and viscosity of the sponge were estimated. Although the shear viscosity of the sponge increased with water content, the increase in shear elasticity was subtle. Because of the limited data set included in this paper, further studies will be performed on a wide range of sponge stages and at more shaker frequencies. Experiments on *ex vivo* swine lungs will also be performed to confirm the results.

Acknowledgments—This work is funded by National Institutes of Health R01 HL 125234. The authors thank Boran Zhou for assisting in the experiments.

REFERENCES

Bluthgen C, Sanabria S, Frauenfelder T, Klingmuller V, Rominger M. Economical sponge phantom for teaching, understanding, and researching A- and B-line reverberation artifacts in lung ultrasound. J Ultrasound Med 2017;36:2133–2142.

Cardinale L, Priola AM, Moretti F, Volpicelli G. Effectiveness of chest radiography, lung ultrasound and thoracic computed tomography in the diagnosis of congestive heart failure. World J Radiol 2014;6:230–237.

Coiro S, Rossignol P, Ambrosio G, Carluccio E, Alunni G, Murrone A, Tritto I, Zannad F, Girerd N. Prognostic value of residual pulmonary congestion at discharge assessed by lung ultrasound imaging in heart failure. Eur J Heart Fail 2015;17:1172–1181.

Corradi F, Brusasco C, Vezzani A, Santori G, Manca T, Ball L, Nicolini F, Gherli T, Brusasco V. Computer-aided quantitative ultrasonography for detection of pulmonary edema in mechanically ventilated cardiac surgery patients. Chest 2016;150:640–651.

Gargani L. Lung ultrasound: A new tool for the cardiologist. Cardiovasc Ultrasound 2011;9:6.

Lichtenstein D, Mezière G. A lung ultrasound sign allowing bedside distinction between pulmonary edema and COPD: The comet-tail artifact. Intensive Care Med 1998;24:1331–1334.

Molinari F, Madhuranthakam AJ, Lenkinski R, Bankier AA. Ultrashort echo time MRI of pulmonary water content: Assessment in a sponge phantom at 1.5 and 3.0 Tesla. Diagn Interv Radiol 2014;20:34–41.

Picano E, Frassi F, Agricola E, Gligorova S, Gargani L, Mottola G. Ultrasound lung comets: A clinically useful sign of extravascular lung water. J Am Soc Echocardiogr 2006;19:356–363.

Picano E, Pellikka PA. Ultrasound of extravascular lung water: A new standard for pulmonary congestion. Eur Heart J 2016;37:2097–2104.

Pivetta E, Goffi A, Lupia E, Tizzani M, Porrino G, Ferreri E, Volpicelli G, Balzaretti P, Banderali A, Iacobucci A, Locatelli S, Casoli G,

Stone MB, Maule MM, Baldi I, Merletti F, Cibinel GA, Baron P, Battista S, Buonafede G, Busso V, Conterno A, Del Rizzo P, Ferrera P, Pecetto PF, Moiraghi C, Morello F, Steri F, Ciccone G, Calasso C, Caserta MA, Civita M, Condo C, D'Alessandro V, Del Colle S, Ferrero S, Griot G, Laurita E, Lazzero A, Lo Curto F, Michelazzo M, Nicosia V, Palmari N, Ricchiardi A, Rolfo A, Rostagno R, Bar F, Boero E, Frascisco M, Micossi I, Mussa A, Stefanone V, Agricola R, Cordero G, Corradi F, Runzo C, Soragna A, Sciullo D, Vercillo D, Allione A, Artana N, Corsini F, Dutto L, Lauria G, Morgillo T, Tartaglino B, Bergandi D, Cassetta I, Masera C, Garrone M, Ghiselli G, Ausiello L, Barutta L, Bernardi E, Bono A, Forno D, Lamorte A, Lison D, Lorenzati B, Maggio E, Masi I, Maggiorotto M, Novelli G, Panero F, Perotto M, Ravazzoli M, Saglio E, Soardo F, Tizzani A, Tizzani P, Tullio M, Ulla M, Romagnoli E. Lung Ultrasound-implemented diagnosis of acute decompensated heart failure in the ED: A SIMEU Multicenter Study. Chest 2015;148:202–210.

Sakka SG, Klein M, Reinhart K, Meier-Hellmann A. Prognostic value of extravascular lung water in critically ill patients. Chest 2002;122:2080–2086.

Soldati G, Giunta V, Sher S, Melosi F, Dini C. "Synthetic" comets: A new look at lung sonography. Ultrasound Med Biol 2011;37:1762–1770.

Zhang X. Identification of the Rayleigh surface waves for estimation of viscoelasticity using the surface wave elastography technique. J Acoust Soc Am 2016;140:3619.

Zhang X, Qiang B, Hubmayr RD, Urban MW, Kinnick R, Greenleaf JF. Noninvasive ultrasound image guided surface wave method for measuring the wave speed and estimating the elasticity of lungs: A feasibility study. Ultrasonics 2011;51:289–295.

Zhang X, Osborn T, Kalra S. A noninvasive ultrasound elastography technique for measuring surface waves on the lung. Ultrasonics 2016;71:183–188.

Zhang X, Osborn T, Zhou B, Meixner D, Kinnick RR, Bartholmai B, Greenleaf JF, Kalra S. Lung ultrasound surface wave elastography: A pilot clinical study. IEEE Trans Ultrason Ferroelectr Freq Control 2017;64:1298–1304.

Zhang X, Zhou B, Kalra S, Bartholmai B, Greenleaf J, Osborn T. An ultrasound surface wave technique for assessing skin and lung diseases. Ultrasound Med Biol 2018;44:321–331.